



Experimental Investigation of a Small-Scale Parabolic Trough Concentrated Solar Power Systems

Ismael EHTIWESH* *Sabratha University, Faculty of Engineering, Department of Mechanical Engineering, Sabratha, Libya*

Highlights

- The developed model may be useful in thermal applications operating at moderate temperatures.
- The performance of small-scale CSP systems is highly affected by wind speed.
- The use of the insulating cavity proved effective in reducing heat loss.

Article Info

Received: 08 Jun 2023
Accepted: 10 Nov 2023

Keywords

Concentrated solar power,
Small-scale power generation,
Parabolic trough,
Solar tracking

Abstract

Large-scale systems have a lower levelized cost of electricity than small-scale concentrated solar power systems. Thus, the purpose of the present study is to evaluate the potential of using standalone small-scale concentrated solar power collectors in order to generate process heat at a moderate temperature, which directly utilizes thermal energy without the need to generate electricity. A parabolic trough collector (3.6m²) was designed and manufactured, including a dual-axis solar tracking system with and without an insulating function. An insulating cavity was incorporated to minimize the heat losses collected by the absorbed tube. The experiments were carried out during a time of high winds and unfavorable weather in Sabratha City. The findings of the experiments demonstrated that the produced temperature and the collected heat energy progressively increase until they reach their maximum value, and then gradually decrease. The maximum water temperature was 96°C at a flow rate of 0.5L/min, and the highest amount of heat energy was 550W/m². Wind speed showed an important impact on the produced temperature; therefore, various comparative experiments were carried out in the same climate condition; the experiment with the insulating function presented the least heat loss, and it takes a higher edge of 11% in terms of efficiency. In addition, the water temperature rose to 120°C where steam was generated at a zero flow rate, while the oil reached 194°C. In addition, a mathematical model was also implemented to theoretically study energy balance; with little expected discrepancy, its predictions and the experimental results agreed. In conclusion, the results presented reasonable markers of interest despite the poor environmental conditions during the experiments.

1. INTRODUCTION

Concentrated solar power systems (CSP) is a technology that transforms beam radiant into thermal energy, and centralize power generating involves a variety of energy conversions. CSP systems covers a number of various types; the common technologies are parabolic troughs, power towers, linear Fresnel, and parabolic dishes [1]. The use of small scales CSP still faces a high value of the Levelized Cost of Electricity compared to large-scale systems, therefore, the goal of this study is to evaluate the viability of small-scale CSP by utilizing the thermal energy collected directly for thermal uses rather than generating electricity. Odeh et al. [2] carried out a design, testing, and evaluation of a single-axis solar tracking parabolic collector with a storage unit at cold wet (latitude 45°) and hot arid (latitude 25°) sites. The average efficiency of the system is about 60%, which is an acceptable comparison with advanced collector efficiency (60-67%) [3]. Said's [4] study addressed an experimental and numerical analyses regarding the solar water heaters in Algeria during the winter using a 1.5-meter Linear Fresnel collector. Findings presented a discernible convergence between the experiment and the numerical results, where optical efficiency is about 43 %, and the equivalent of 545.68 kWh of electrical capacity. Economically, the system cost is 378.87 \$, which is recoverable in about 16 years, the system provided the equivalent of 127.47 m³ of Liquefied natural gas. Göttsche et al.'s [5] study presented a portion of the heliostat's expense is attributable to the steel structure's

*e-mail: ismael.ehtiwesh@sabu.edu.ly

high stiffness requirement, typically yielding 20 kg/m² of steel per mirror area with price of 150 €/m² that is due to an increase in the price of raw materials. Small mirrors with a size of 10x10 cm were placed in a square frame with a dimension of 0.5 x 0.5 m. Therefore, to reduce the heliostat costs, drives and mechanical layouts were kept less robust by shielding all moving parts from wind loads. The possibility of a low cost is offset by around 40%, but less optical performance. Ehtiwesh's [6] study developed a small-scale concentrated solar power model using central receivers technology, which uses thermal energy directly, with particular emphasis on the use of solar cooking. The sun's rays are reflected using 56 small mirrors and focused on the bottom of the cooking pot. The study involves the design and manufacture, a solar tracking system, and experimental analysis. The area of the proposed model is 1 m², while the heliostat area is 0.56 m². The findings were excellent and suggested a possible interest. A half-liter of water took 20 minutes to heat up to the point of starting to boil, and 193°C was the oil's highest measured temperature. Saldivar-Aguilera et al.'s [7] study implemented a single-axis solar tracking system's technique considering 10 m² parabolic trough collector. It integrated the signals of photodiodes solar with a shadow-based visual detection unit in order to minimize the tracking error. The errors for both photodiodes and the proposed dual control were ±0.82° and ±0.11°, respectively. This divergence in error implies an 80% reduction in the error and provides a 15% increase in the thermal efficiency. Loni et al.'s [8] study utilized a parabolic trough collector with a linear cubical cavity receiver using thermal oil as a heat transfer fluid. The measured thermal and developed model efficiencies showed an interesting agreement. Several cavity geometrical parameters including the cavity's position, aperture, height, and cavity tube diameter were tested. Reductions in tracking and optical errors are correlated with improved optical performance, and when the ideal cavity depth is equal to the cavity aperture width. In addition, the cavity must be placed in the parabola's focus line; the thermal efficiency is approximately 77% where a cavity tube diameter was 5 mm. The study [9] developed a numerical model for a parabolic collector within a linear V-shape cavity considering several dimensional and operational parameters. The results showed that the highest optical performance could be obtained when the cavity was positioned at the focal line. The optimal performance was found at a low inlet temperature, high beam radiation level, and smaller cavity tube diameter. The study [10] investigated an experimental study using a particular cavity receiver for a 2-meter parabolic trough collector. A center tube and two inclined fins use to absorb the reflected solar energy. The prototype efficiency ranges between 34% and 48%, and there is a great deal of room for performance improvement with the cavity receiver. In the study [11], the design and fabrication of a 0.65 m² parabolic collector were conducted at the same location under study (Sabratha, Libya). The frame was made of wood, and a sheet of silver was used as a reflector. The maximum gained efficiency and heat energy were about 53% and 248W/m², respectively. The same prototype was optimized in the study [12] using a stainless steel reflector, and copper absorbed-tube, the efficiency was increased by 2.26%. Despite the region offering good outstanding conditions for CSPs implementation [13], the study [12] indicates that the impact of the wind speed on the collector performance is high, which is due to the absence of the enveloping vacuum tube that can minimize the heat loss. This present work aims to address the potential of utilizing a standalone small-scale concentrated solar power collector in order to generate process heat at a reasonable temperature, utilizing a parabolic trough technology, which incorporates the most proven and widely used technology [14]. The study incorporates the important concerns outlined in studies [11, 12], in order to create the following prospective improvements: 1) the receiver area is double of the previous model, 2) a dual-axis solar tracking system that can be used along the year were developed, while the previous model used one axis orientation and it can only be used around October, 3) create a thermal insulator (cavity) with the intention of reducing heat losses in order to improve the performance of the collector. In addition, a theoretical mathematical model was used in addition to the practical trials to assess heat losses and performance patterns.

2. DESIGN SCOPE

The present study considers the processes of design, fabrication, dual-axis solar tracking, testing, and evaluation of a standalone small-scale parabolic trough collector. The developed collector consists of several components as illustrated in Figure 1, namely, 1) the fixed steel base that couples with 2) the rotating steel frame, using two bearings type 205-UC, this frame carries 3) the reflector that consists of 6 parts to carry two steel flat sheets (1-meter width each); the sheets are formed to parabolic shape and covered within a thin silver sheet, 4) the receiver is mounted on at the focal line within adjustable supports, it consists of

an absorbed copper tube, which is sprayed with a black coating and inserted inside a rectangular casing (the cavity) that insulated at the top inside with thermal resistance silicon and at the bottom with a single glazed opening and 5) a closed loop tracking unit.

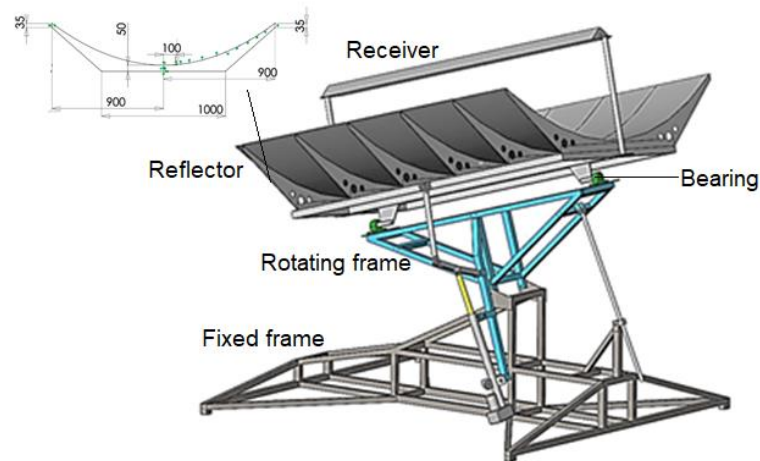


Figure 1. Geometry of the developed parabolic trough collector (Dimensions in mm)

The beam radiation is received by the parabolic surface and reflected on a focal line of the copper-absorbed tube; the reflector has dual-axis rotation, automated from East to West by around 240° , and manually from North to South. In the nominal design parameters, the collector length is assumed 2 meters, and the aperture width is 1.8-meters; therefore, the total area of the reflector is 3.6 square meters. The geometrical aspects of the parabola are shown in Figure 2; the aperture area is calculated by the product of the aperture's width and the collector length. The incident angle θ_m is the angle at which the solar beams hit the collector. The focal length ($f=0.6$ meters) is the vertical distance from the vertex to the focus of the parabola. The focal length is designed based on the insulating cavity dimensions, where the width of the solar flux pattern in the focal line is used to determine the cavity's width [2]. The cavity is a rectangular tube (10 x 5 cm) with a single glazed opening at the bottom side, and the absorbed copper tube with a diameter of 2.1 cm and 0.1 cm thickness.

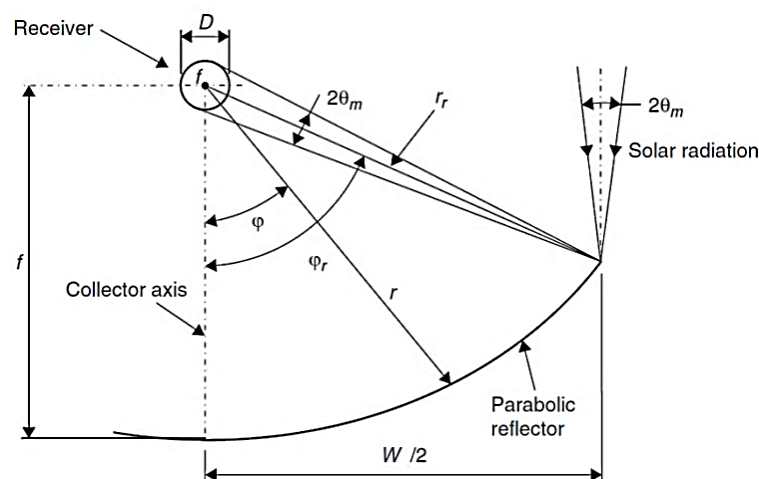


Figure 2. Cross-section of a parabolic trough collector [15]

The incident radiation creates an angle ϕ_r on the reflector at the collector's rim where the reflector radius r_r has the maximum value, with the collector's center line (rim angle). The parabola's equation using the coordinate system is given as follows:

$$y = x^2/4f. \quad (1)$$

The diameter of the absorbed tube must be precisely selected to intercept every solar image

$$D = 2r_r \sin(\theta_m) \quad (2)$$

where θ_m is a half acceptance angle and the radius can be calculated as follows:

$$r = 2f/1 + \cos(\varphi) \quad (3)$$

where φ is the angle between a reflected beam at the focus and the collector axis, and calculated φ_r is 74° . Table 1 reported the design and real prototype dimension of the parabola.

Table 1. Design and real dimensions of the parabola

x (m)	0	0.1	0.2	0.3	0.4	0.5	0.6	0.7	0.8	0.9
y _{Disgn} (m)	0	0.004	0.017	0.038	0.067	0.105	0.151	0.205	0.268	0.339
y _{Right} (m)	0	0.002	0.011	0.030	0.061	0.100	0.149	0.201	0.266	0.335
y _{Left} (m)	0	0.001	0.025	0.035	0.072	0.108	0.160	0.220	0.279	0.370

The production and assembly of the prototype are the goals of the subsequent step, where the parabolic parts that will support the parabolic collector sheet are depicted in Figure 3, where Figure 4 presents the fixed steel base that couples by bearing with the rotating steel frame.



Figure 3. Manufacturing and assembly of the developed prototype' frame



Figure 4. The real developed collector

3. TRACKING SYSTEM

One of the most crucial elements for increasing the efficiency of concentrated solar power systems is the sun tracking system. The selection of tracking axis configuration is based on site latitude and solar irradiation. The developed prototype has a dual tracking axis, namely, 1) a manual North-South tracking axis that typically uses seasonally and 2) an automated East-West tracking axis that integrates the signals from a photodiode solar sensor. A closed-loop control system is employed to follow the sun around the East-West axis. The tracking unit used in this study encompasses a set of devices and accessories as depicted in Figure 5, namely, a) Displacement actuator (36V), b) Power supply, c) Light-dependent resistors (LDRs – $1M\Omega$) and d) ESP32 board (260Mhz, 520kB).

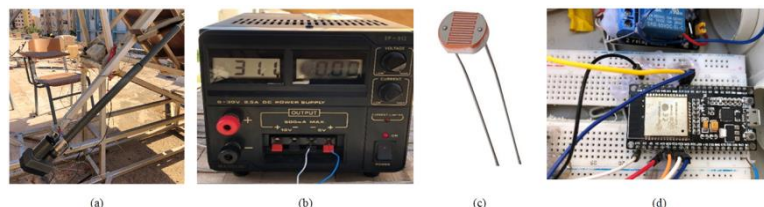


Figure 5. Tracking system elements

Two LRDs are located on either side of the reflector, when the solar beam plane is perpendicular to the collector aperture, both LRDs should have approximately the same resistance. Any change in the sun's position (the incident angle will be changed) will cause different beam intensities, thus, leading to different resistance. The different resistance is used as part of a Wheatstone bridge circuit to provide zero voltage when the different resistance value is around zero, i.e. the sun is in the center of the parabola. The sensors

provide a voltage proportional to that change when the sun's position changes. The controller amplifies the voltage and sends a signal to the actuator motor to rotate the reflector by keeping the Wheatstone bridge voltage equal to zero. LRD does not distinguish between direct radiation and diffuse radiation; therefore, a third modulation LRD is used that can be positioned for direct radiation to reduce the solar tracking error.

4. EXPERIMENTS

A set of experiments was carried out to evaluate the developed model at Sabratha site (Latitude 32.8° N, Longitude 12.4° E). The location has a suitable DNI for concentrated solar energy applications, where the daily average is around 1000 W/m² during the summer and 350 W/m² during the winter, and the average daily temperatures range between 5 and 45 °C [16]. The experiments were carried out between 12:00 and 14:00, the solar radiation, ambient temperature and wind speed were measured at every test, the inlet and outlet temperatures were recorded automatically every five minutes, and water was used as a heat transfer fluid. The experiments were carried out during the time period from 08-Nov-2022 to 18-Nov-2022; due to the climate was unsuitable for conducting the experiments, consequently, this period is probably going to witness the lowest performance of the year. The preliminary experiment was carried out with no water flow (static state) on 08-Nov-2022; in a short time (12 minutes) the water passed the boiling point (100°C), and a few minutes later water temperature reached 120°C and steam was generated as depicted in Figure 6. The ideal north-south tilt angle was established and maintained throughout this experiment, wherein during the remaining experiments, the automated tracking procedure is carried out from east to west. The purpose of the subsequent experiment was to find the most practical flow rate by varying the flow rate with a bypass return line from 0.3 to 1 L/min in order to attain the highest possible temperature. The water outlet temperature was nearly equal to the inflow temperature at flow rates greater than 0.7 L/min, therefore, the following tests were implemented using 0.5 L/min.



Figure 6. Steam generated at zero flowrate test

Devices and accessories used in the experiments are presented in Figure 7: a) A Pyrometer (Type CMP6) that uses to identify the direct normal irradiation, b) Anemometer to measure the wind speed, c) Flowmeter to control the heat transfer fluid (HTF) flow, d) Thermocouples to measure the HTF' temperature inside the absorbed tube and e) pump and 20L reservoir

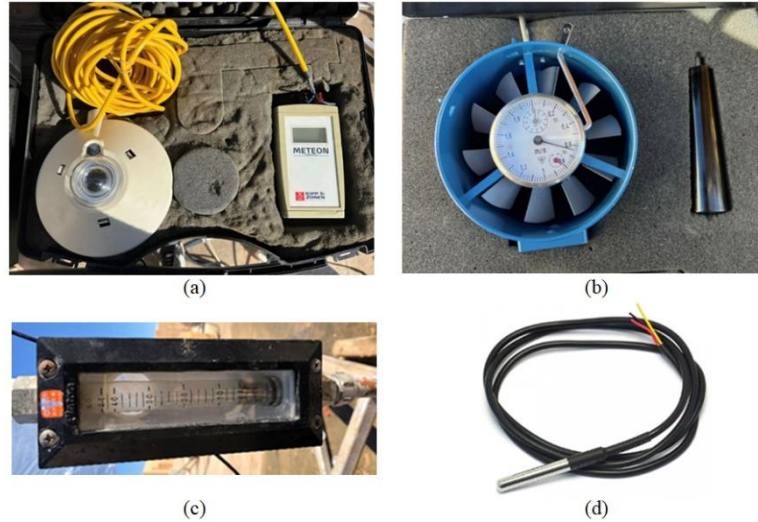


Figure 7. Devices and accessories used in the experiments

To verify the consistency of the experimentally observed data, uncertainty analysis was used. In order to evaluate the uncertainty, numerous sets of data collected throughout the experiment are used, which makes it possible to determine whether the experimental results can be duplicated. The measuring device and measurement repetition uncertainties lead to the total uncertainty. Equations (4) – (6) allow for the calculation of the parameter's overall degree of uncertainty [17] as given as follows:

$$U_{total} = \sqrt{(U_{rep})^2 + (U_{eqp})^2} \quad (4)$$

where U_{total} is the total uncertainty, U_{rep} is the repetition uncertainty and U_{eqp} is the equipment uncertainty.

$$U_{rep} = S_d / \sqrt{P} \quad (5)$$

$$U_{eqp} = a / \sqrt{3} \quad (6)$$

where, S_d is the standard deviation, P is the number of repeated measurements, and a is half of the equipment accuracy. Information on the pieces of equipment used for the experimental measures is listed in Table 2, including their range, resolution, accuracy, and total level of uncertainty. It clearly shows that the experiments' total level of uncertainty is low.

Table 2. The measured parameters' uncertainty

Parameter	Equipment	Measuring range	Resolution	Accuracy	U_{total}
Temperature	Thermocouple	0-300 °C	0.1 °C	± 0.1 rdg 0.5 °C	± 0.34
Solar radiation	Pyranometer	0-2000 W/m ²	1 W/m ²	± 1%	+ 4
Wind speed	Anemometer	0-70 m/s	0.1 m/s	± 1%	+ 0.09

The experimental thermal efficiency of the collector (η_{exp}) can be determined using the ratio of the conversion of thermal energy from the collector to useful radiation [18], i.e. the collected beams falling on the reflector surface.

$$\eta_{exp} = \dot{m}C_p(T_{out} - T_{in})/DNI A_p \quad (7)$$

where DNI is the direct normal irradiation (W/m^2), A_p is the collector aperture area. The first experiment was carried out on 13-Nov-2022 without the use of the insulating cavity; Figure 8 demonstrates the collector efficiency and water outlet temperature. The speed of wind during this experiment varies between 0.6 and 2.2 m/s, while the solar radiation ranges between 600 and 691 W/m^2 . On November 16, the second experiment was carried out employing the insulating model; Figure 9 shows the collector efficiency and water outlet temperature. The wind speed during this experiment varies between 1.5 and 3.2 m/s, while the solar radiation ranged between 524 and 673 W/m^2 .

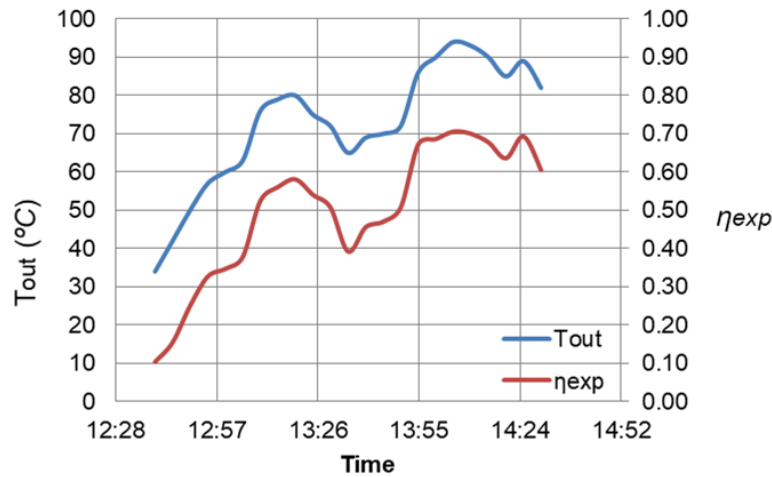


Figure 8. The collector efficiency and outlet temperature on 13 Nov without insulating function

It can be noted that there is a linear relationship between thermal efficiency and the outlet temperature, which is expressed in Equation (7), due to the reservoir is in an opening environment without insulation, the inflow temperature increases slightly; therefore, the efficiency increases with an increase in ΔT as shown in Figure 10, and this is why the efficiency is high. The observed fluctuation in Figure 8 is mainly a result of the instability in wind speed demonstrated in Figure 11; meanwhile, in Figure 9, the use of insulation has led to smooth behavior. It should be mentioned that during each experiment, the solar radiation slightly changes, i.e. almost constant. The collector efficiency with the use of the insulating presented in Figure 9 is higher than that presented in Figure 8 (no insulating) by approximately 13%.

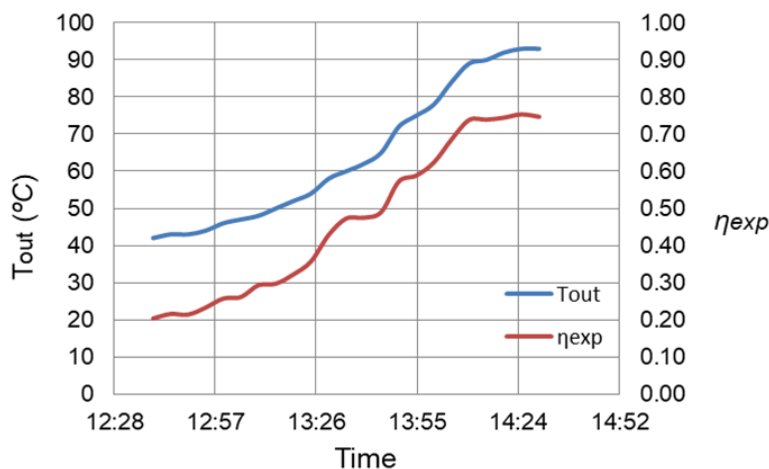


Figure 9. The collector efficiency and outlet temperature employing insulating model on 16 Nov

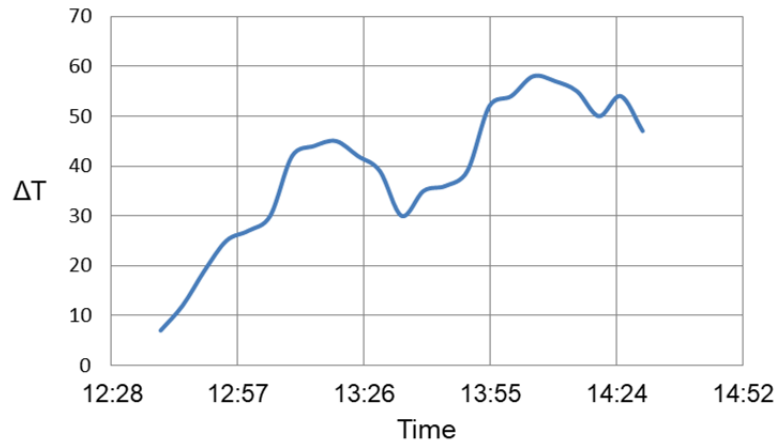


Figure 10. Differences in temperature between inlet and outlet (ΔT)

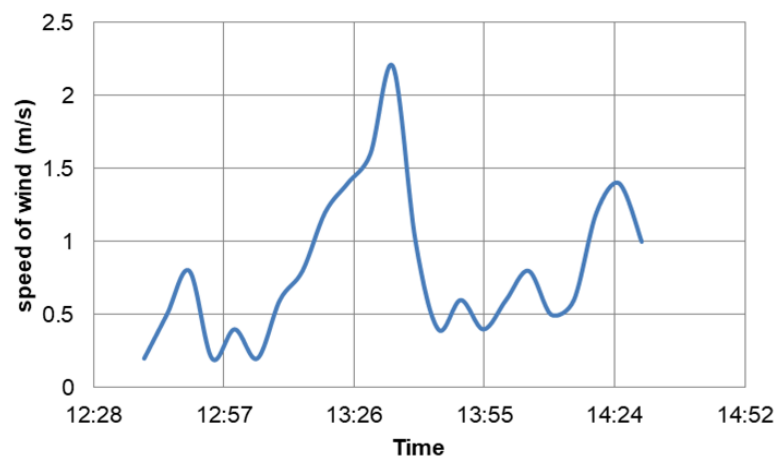


Figure 11. Speed of wind variation during the experiment conducted on 13 Nov.

In order to illustrate how the insulating model reduces heat loss and improves thermal efficiency, two additional experiments were conducted on the same day, November 17; the wind speed was high and the sky was mostly cloudy. The experiments were conducted with and without the insulating model; the results were shown in Figures 12 and 13, respectively. During these tests, the wind speed ranged from 2.4 to 3.9 m/s, while the solar radiation ranged between 612 and 642 W/m².

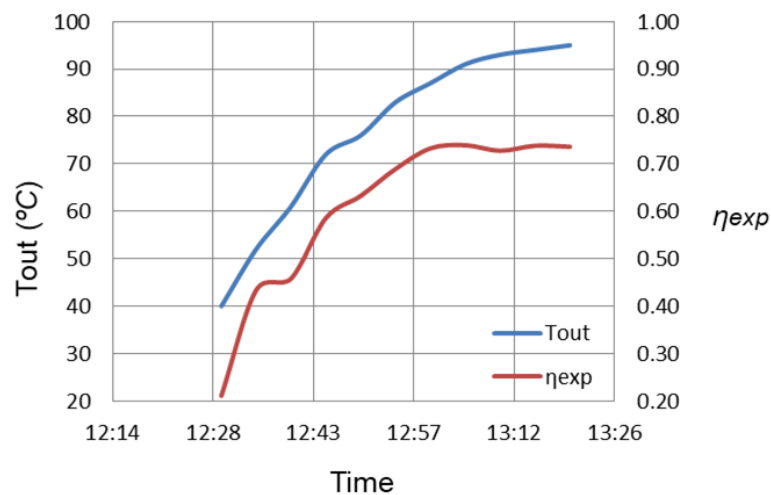


Figure 12. The collector efficiency and outlet temperature with insulating model on 17 Nov.

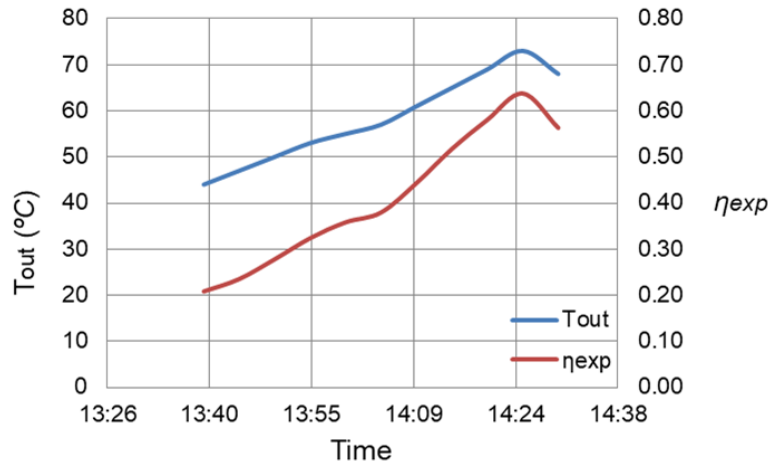


Figure 13. The collector efficiency and outlet temperature without insulating model on 17 Nov.

Despite the unfavorable climatic conditions, the wind speed was about 3 m/s, the thermal efficiency using the insulator reached 74% as shown in Figure 12, and the highest temperature is 95°C. The maximum efficiency was 63% when insulation was not used as Figure 13 illustrates; the highest outlet temperature was 73 °C at a wind speed of about 3.1 m/s. The latest experiment was carried out on 18-Nov-2022 using corn oil instead of water without insulation and flow rate is zero. The wind speed ranged between 3.5 and 3.9 m/s, in 18 minutes the oil temperature reached 194°C, and then it remained there, most likely because of the wind speed and nearby scattered clouds.

Table 3 compares small-scale parabolic trough solar collector literature regarding the maximum produced temperature and collector area.

Table 3. Comparison with small-scale parabolic collectoes studies

Study	Function	Max temp °C	Area m ²	Working fluid
Present study	Education	195 100	3.6	Corn oil Water
[19]	heating	80	1.5	water
[20]	heating	110	1	water
[21]	cooking	265	1.3	Thermal oil
[22]	cooking	118.4	0.445	Air
[9]	Education	185	1.4	Thermal oil

5. ENERGY BALANCE MATHEMATICAL MODEL

The heat transfer fluid is heated by concentrating solar energy before flowing into a heat exchanger through a "hot" header tube, where forced convection is used to transfer the heat. A cold header pipe directs the heat transfer fluid that exits the collector to the reservoir. The absorber tube surface is intended to absorb the solar energy that the reflector reflected on the receiver tube. Part of this energy transfers to the heat transfer fluid by forced convection, whereas the remaining energy is either lost through the brackets or transmitted back to the cavity envelope case by radiation and natural convection [16]. The heat loss in the absorber takes the form of radiation and natural convection, and the absorbed radiation is considered as a heat flux term [23]. The produced power depends on the heat transfer, mass flow and temperature. Heat losses from the absorbed pipe to the cavity casing, and from the cavity casing to the surrounding air, are influenced by difference in temperature between the heat transfer fluid and ambient temperatures. The optical losses are caused by tracking mistakes, shadowing, and flaws in the collector surface. The heat lost by the brackets ranges approximately between 1 and 4 % out of total losses, depending on the surrounding conditions and heat transfer fluid' temperature [13]. A straightforward model based on the energy balance using the thermal resistance model depicted in Figure 14 is to be used in accordance with the convection and radiation

measurements between the outermost receiver surface and the ambient with and without insulating cases. The heat loss (q_l) is assumed to calculate for both cases as follows:

$$q_l = q_{conv,amb} + q_{rad,sky} + q_{bracket} \quad (8)$$

where $q_{conv,amb}$ and $q_{rad,sky}$ are the heat transferred from the outer cavity surface to the surrounding ambient by convection and radiation, respectively, and $q_{bracket}$ is the conductive losses by the brackets.

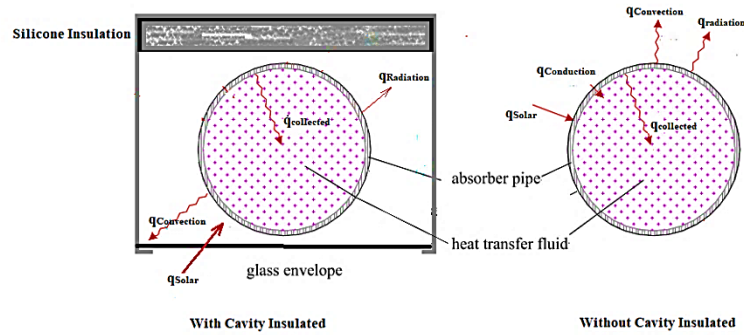


Figure 14. The receiver thermal resistance network

In this work, the brackets losses are considered to be 4% of the total losses [13], the radiation heat transfer from the outer surface of the receiver to the atmosphere is given by [24]:

$$q_{rad,sky} = \sigma \cdot \epsilon_g \cdot \pi \cdot D_{tube} \cdot l_{tube} (T_{tube,out}^4 - T_{sky}^4) \quad (9)$$

where T_{sky} is the temperature of the sky and T_{tube} is the temperature of the envelope's outer surface. According to Forristall [23], $q_{rad,sky}$ is comparatively unaffected by changes in the reflector's view factor and the reflector's temperature; typically, using insulating model, the relation between the sky and ambient temperatures is ($T_{sky}=T_{atm}-8$) in °C [25]. ϵ_g is the emissivity of the envelope outer surface and σ is the Stefan-Boltzmann constant. Newton's law of cooling defines the convection heat transfer from the surface of the outer envelope to the ambient:

$$q_{conv} = h_{conv} \cdot \pi \cdot D_{tube} \cdot l_{tube} (T_{tube,out} - T_{amb}) \quad (10)$$

where h_{conv} is the convective heat transfer coefficient to ambient, and is calculated using the following formula, which is greatly influenced by wind speed.

$$h_{conv} = (k_{th}/D_{tube}) \cdot Nu_{air} \quad (11)$$

Nu_{air} is the average Nusselt number based on the outside diameter of the envelope tube (D_{tube}) [24] and k_{th} is the air thermal conductivity $(T_{tube} + T_{amb})/2$. The Nusselt number depends on whether the convection heat transfer is natural (with insulated cavity) i.e. that there is no wind effect, or forced (with insulated cavity) where a considerable wind effect exists, as follows:

1. With insulating cavity

$$Nu_{air} = \left\{ 0.6 + 0.387 Ra_{air}^{1/6} / [1 + (0.559/Pr_{air})^{9/16}]^{8/27} \right\}^2 \quad (12)$$

where Pr_{air} and Ra_{air} are air Prandtl number and the Rayleigh number, respectively.

$$Ra_{air} = g\beta(T_{tube,out} - T_{amb}) / (\alpha_{air} \nu_{air}) \quad (13)$$

where ν_{air} is the air kinematic viscosity, β is the volumetric thermal expansion coefficient ($1/K$), α_{air} is thermal diffusivity of the air and T_{amb} is the average temperature inside the insulated cavity. The top wall is considered to be well-insulated, thus the thermal loss from the insulating cavity's internal ambient to the atmosphere is ignored; for example, fiberglass blanket insulation (0.035 W/m-K) with 0.05 m thickness results in a typical reduction in heat loss of about 90% . [26].

2. Without insulating cavity

$$Nu_{air} = CR_e^m Pr^{1/3} \quad (14)$$

where Re is Reynolds number that depends on wind speed, and Prandtl numbers is widely used for $Pr \geq 0.7$ [24], the constants C and m are provides in [24]. The heat energy from the sun that collected by the HTF circulates in one meter of the absorber tube is known as the absorbed heat (q_a). It is influenced by a fraction of direct solar beam corrected for incidence angle, row shadowing, the availability of solar fields, the cleanliness of the collector and the collector's surface characteristics; and calculated by the following relation:

$$q_a = DNI \cdot IAM \cdot \cos \theta_m \cdot \eta_{opt} \cdot A_p \quad (15)$$

where θ_m is the incidence angle, η_{opt} stands for optical efficiency at normal incidence, which takes into account the reflector's reflectance, the glass envelope's transmittance, the absorber's absorption, as well as the effects of shade, dirt and geometry [27]. IAM is the incidence angle modifier, a function of the collector incidence angle and the optical quality and it is calculated as given [28]:

$$IAM = \min(1, \cos \theta_m + 0.000884 \cdot \theta_m - 0.0000537 \cdot \theta_m^2 / \cos \theta_m). \quad (16)$$

The useful heat collected by the heat transfer fluid (q_c) is the difference between the absorbed heat and the lost heat

$$q_c = q_a - q_l. \quad (17)$$

The collector theoretical thermal efficiency can be determined by the follows:

$$\eta_{th} = q_c / DNI A_p. \quad (18)$$

Figure 15 illustrates the theoretical impacts of wind speed on the efficiency where the solar radiation is kept constant at 400 W/m^2 without the employment of insulation. Figure 16 shows the effect of ambient temperature on the efficiency with and without the employment of insulation.

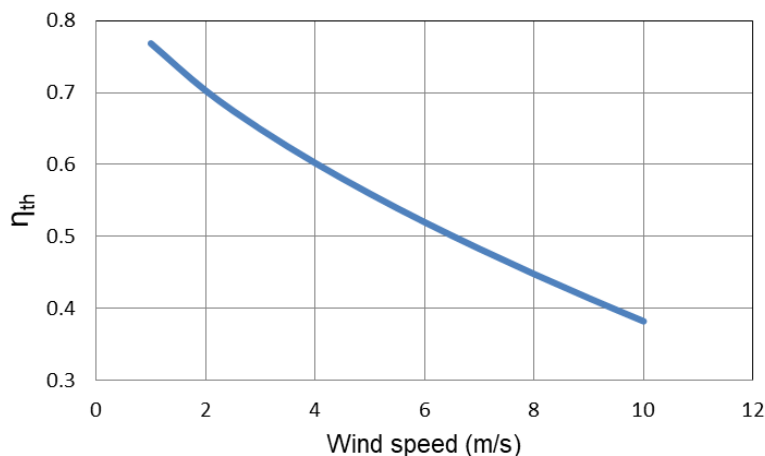


Figure 15. The heat losses and collector efficiency variation with wind speed at 400 W/m^2

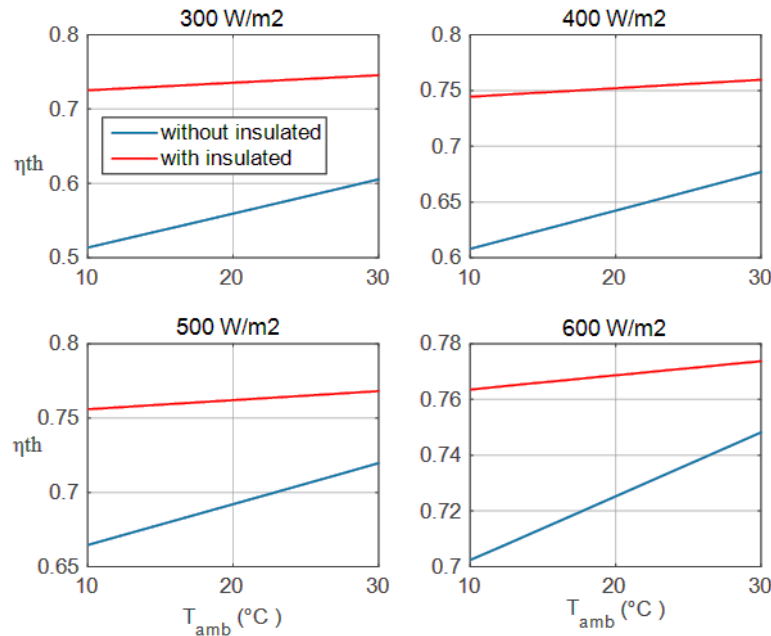


Figure 16. The ambient temperature effect on the collector efficiency with and without insulating at various radiations

It can be noted that the ambient temperature has a negligible impact on the collector efficiency and wind speed has an important effect. It is evident that adding an insulation cavity increases collector efficiency by more than 20%. High solar radiation significantly enhances the collector's efficiency when it doesn't have an insulating cavity and slightly improves it when the insulating is used. Figure 17 demonstrates the theoretical efficiency comparison with the experimental efficiency that was conducted on 13-Nov-2022, where the same experimental conditions were used.

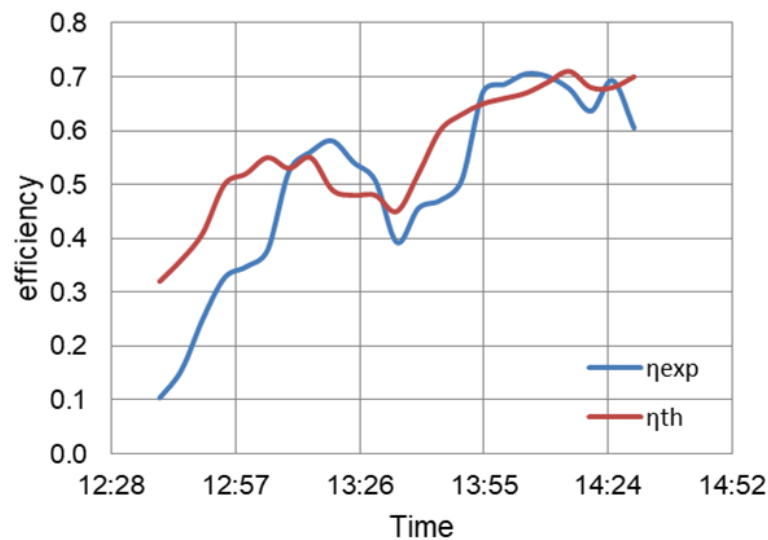


Figure 17. Comparison results of experimental and theoretical efficiencies

The experimental results are consistent with the theoretical predictions, with expected disparity can be noted, which is due to several reasons such as 1) the effect of ΔT on the experimental efficiency, 2) the mathematical model does not account for some parts of loss, 3) theoretical predictions are independent of one another (Each record's calculation was done separately), 4) the reflector surface's absorption and reflectivity make them ineffective as mirrors and 5) the manufacturing error in reflector surface and receiver position.

6. CONCLUSION

Parabolic trough collector with area of 3.6 m² was designed and manufactured taking into consideration the employment of a dual-axis sun tracking system and the insulating cavity that aims to reduce heat losses. A mathematical model was also implemented to analyze heat losses and performance behaviors. The experiments were conducted at the Sabratha site during windy and unfavorable weather conditions. The findings of the experiments demonstrated that the produced temperature and the collected heat energy progressively increase until they reach their maximum value between 13:00 and 14:30, and then gradually decrease, regardless of the fluctuations brought on by fluctuating wind speeds in scenarios where the insulation cavity was not employed. The following is a list of conclusions:

- The maximum outlet temperature of the water was 96 °C at 0.5L/min, and the highest heat energy was 550W/m²; where the outlet temperature is highly affected by wind speed. Consequently, the use of the insulator proved successful in reducing heat loss, so the outlet water temperatures and collected thermal energy were higher. The highest collector efficiency with and without insulating was about 74% and 63%, respectively.
- The maximum temperature at zero flowrates using water were 120°C where the steam was generated, and for oil 194°C. The mathematical model predictions are well agreed with the experimental behavior with little expected disparity.
- In conclusion, results presented reasonable markers of interest despite the poor environmental conditions during the experiments and the reflector surface was not typical. Therefore, in future work, the research order assumes to utilize a parabolic mirrors and glass enveloping tubes in order to witness a promising improvement in performance.
- Finally, due to large-scale systems having a lower levelized cost of electricity than small-scale concentrated solar power systems. This study aimed to study the potential of using small-scale collectors to generate process heat at a moderate temperature that directly uses thermal energy without the need to generate electricity. A prototype (3.6m²) was designed and manufactured with a dual-axis solar tracking system and insulation cavity. The design can be useful for several thermal applications that can operate at a moderate temperature, such as heating, storing thermal energy, educational assessments and in particular for domestic use.

CONFLICTS OF INTEREST

No conflict of interest was declared by the authors.

ACKNOWLEDGMENTS

Manufacturing implementations of the developed prototype were carried out in the Department of Mechanical Engineering workshop, Faculty of Engineering, Sabratha University. The author also gratefully acknowledges the bachelor's students: A. Mansor, M. Sultan, M. Omar, and M. Almadnini for their contribution to conducting this work.

Nomenclatures

A_p	Aperture area
C_p	Specific heat capacity
D	Diameter
DNI	Direct normal irradiation
f	Focal length
h	convective heat transfer coefficient
IAM	Incident angle modifier
k_{th}	Thermal conductivity
l	Length
\dot{m}	Mass flow rate
Nu	Nusselt number
P	The number of repeated measurements
P_r	Prandtl number
q	Heat energy

r	radius
R_a	Rayleigh number
R_e	Reynolds number
S	The standard deviation
T	Temperature
U	Uncertainty

Greek symbols

a	A half of the equipment accuracy
θ	Angle
φ	Angle between a reflector beam and collector axis
α	Diffusivity
η	Efficiency
ε	Emissivity
ν	Kinematic viscosity
σ	Stefan-Boltzmann constant
β	Volumetric thermal expansion coefficient

Abbreviations

amb	Ambient
atm	Atmosphere
d	Deviation
eqp	Equipment
exp	Experiment
g	Glass
m	Incident
opt	Optical
r	Reflector
rep	Repetition

REFERENCES

- [1] Montes, M., Abánades, A., Martínez-Val, J., and Valdés, M., “Solar multiple optimization for a solar-only thermal power plant, using oil as heat transfer fluid in the parabolic trough collectors”, *Solar Energy*, 83(12): 2165–2176, (2009).
- [2] Odeh, S. D., and Abu-Mulaweh, H. I., “Design and development of an educational solar tracking parabolic trough collector system”, *Global Journal of Engineering Education*, 15(1): 21–27, (2013).
- [3] Mousazadeh, H., Keyhani, A., Javadi, A., Mobli, H., Abrinia, K., and Sharifi, A., “A review of principle and sun-tracking methods for maximizing solar systems output”, *Renewable and Sustainable Energy Reviews*, 13(8): 1800–1818, (2009).
- [4] Said, Z., Ghodbane, M., Tiwari, A. K., Ali, H. M., Boumeddane, B., and Ali, Z. M., “4E (Energy, Exergy, Economic, and Environment) Examination of a Small LFR Solar Water Heater: An Experimental and Numerical Study”, Elsevier logo Journals & Books Go to journal home page - Case Studies in Thermal Engineering Case Studies in Thermal Engineering, 27(October), 101277, (2021).
- [5] Götttsche, J., Hoffschmidt, B., Schmitz, S., Sauerborn, M., Buck, R., Teufel, E., Badstübner, K., Iffland, D., and Rebholz, C., “Solar concentrating systems using small mirror arrays”, *Journal of Solar Energy Engineering*, ASME, 132(1): 0110031–0110034, (2010).
- [6] Ehtiwesh, I. A. S., “Experimental evaluation for enhancement of small-scale concentrated solar power systems – a case study for solar cooking”, *Energy Sources, Part A: Recovery, Utilization, and Environmental Effects*, 45(4): 11681–11696, (2023).

- [7] Saldivar-Aguilera, T. Q., Diaz-Ponce, A., Valentin-Coronado, L. M., Pena-Cruz, M. I., and Acevedo, R. G. A., "Dual feedback closed-loop control for one-axis solar trackers of parabolic trough collector systems", 2021 23rd IEEE International Autumn Meeting on Power Electronics and Computing, ROPEC, (2021).
- [8] Loni, R., Ghobadian, B., Kasaeian, A. B., Akhlaghi, M. M., Bellos, E., and Najafi, G., "Sensitivity analysis of parabolic trough concentrator using rectangular cavity receiver", *Applied Thermal Engineering*, 169(April 2019), (2020).
- [9] Rafiei, A., Loni, R., Ahmadi, M. H., Najafi, G., Bellos, E., Rajaei, F., and Asli-Ardeh, E. A., "Sensitivity analysis of a parabolic trough concentrator with linear V-shape", *eEnergy Science & Engineering*, 8: 3544–3560, (2020).
- [10] Liang, H., Zhu, C., Fan, M., You, S., Zhang, H., and Xia, J., "Study on the thermal performance of a novel cavity receiver for parabolic trough solar collectors", *Applied Energy*, 222(April), 790–798, (2018).
- [11] Alghol, A., and Karim, M., "Design and fabrication of parabolic trough collector", Sabratha University, Department of Mechanical Engineering, Bs.c project, (2016).
- [12] Ahmed, A., and Moaad, A., "Optimization of parabolic trough collector", Sabratha University, Department of Mechanical Engineering, Bs.c project, (2021).
- [13] Ehtiwesh, I. A. S., Neto Da Silva, F., and Sousa, A. C. M., "Deployment of parabolic trough concentrated solar power plants in north africa – a case study for libya", *International Journal of Green Energy*, (2018).
- [14] Ehtiwesh, I. A. S., Coelho, M. C., and Sousa, A. C. M., "Exergetic and environmental life cycle assessment analysis of concentrated solar power plants", *Renewable and Sustainable Energy Reviews*, 56: 145–155, (2016).
- [15] Kalogirou, S. A., "Solar Energy Collectors", *Solar Energy Engineering Processes and Systems*, Academic Press is an imprint of Elsevier, 125–220, (2014).
- [16] Ehtiwesh, I., Neto da Silva, F., and Sousa, A., "Performance and economic analysis of concentrated solar power plants in Libya", 2nd International Conference on Energy and Environment: Bringing Together Engineering and Economics, ICEE, 18-19 June, Guimarães, Portugal, 459–66, (2015).
- [17] Farzanehnia, A., Khatibi, M., Sardarabadi, M., and Passandideh-Fard, M., "Experimental investigation of multiwall carbon nanotube/paraffin based heat sink for electronic device thermal management", *Energy Conversion and Management*, 179: 314–325, (2019).
- [18] Ghodbane, M., Boumeddane, B., Hussain, F., Zhar, R., Lahrech, K., Bhatti, J., Zhang, B., Yassin, H., De Silva, L. C., and Barbón, A., "Evaluation of the Design and optical errors for a parabolic trough collector field in an algerian desert region: gassi-touil as a study area", *Energy Reports*, 8(November), 15326–15337, (2022).
- [19] Faheem, M., Jizhan, L., Akram, M. W., Khan, M. U., Yongphet, P., Tayyab, M., and Awais, M., "Design optimization, fabrication, and performance evaluation of solar parabolic trough collector for domestic applications", *Energy Sources, Part A: Recovery, Utilization and Environmental Effects*, 1–20, (2020).
- [20] Özcan, A., Devocioğlu, A. G., and Oruç, V., "Experimental and numerical analysis of a parabolic trough solar collector for water heating application", *Energy Sources, Part A: Recovery, Utilization and Environmental Effects*, 44(2): 4184–4203, (2022).

- [21] El Moussaoui, N., Talbi, S., Atmane, I., Kassmi, K., Schwarzer, K., Chayeb, H., and Bachiri, N., “Feasibility of a new design of a parabolic trough solar thermal cooker (PSTC)”, *Solar Energy*, 201(February), 866–871, (2022).
- [22] Harmim, A., Merzouk, M., Boukar, M., and Amar, M., “Performance study of a box-type solar cooker employing an asymmetric compound parabolic concentrator”, *Energy*, 47(1): 471–480, (2012).
- [23] Forristall, R., “Heat Transfer Analysis and Modeling of a Parabolic Trough Solar Receiver”, Implemented in Engineering Equation Solver, National Renewable Energy Laboratory, Technical Report NREL/TP-550-34169, (2023).
- [24] Incropera, F., Bergman, T., Lavine, A., and Dewitt, D., “Fundamentals of Heat and Mass Transfer”, John Wiley & Sons, (2011).
- [25] Burkholder, F., and Kutscher, C., Heat Loss Testing of Schott’s 2008 PTR70 Parabolic Trough Receiver, Technical Report: NREL/TP-550-45633, (2009).
- [26] Ehtiwesh, I. A. S., and Sousa, A. C. M., “Numerical model for the thermal behavior of thermocline storage tanks”, *Heat Mass Transfer*, 54(3): 831–839, (2018).
- [27] Padilla, R., “Simplified methodology for designing parabolic trough solar power plants”, PhD Thesis, University of South Florida, (2011).
- [28] Dudley, E., Kolb, J., Mahoney, R., Mancini, T., Matthews, C., Sloan, M., and Kearney, D., “Test Results: SEGS LS-2 Solar Collector, Report: SAND94-1884”, (1994).